INT. J. REMOTE SENSING, 20 DECEMBER, 2003,
VOL. 24, NO. 24, 5095–5117

Taylor & Francis
Taylor & Francis Group

A new approach for retrieving precipitable water from ATSR2 split-window channel data over land area

ZHAO-LIANG LI†*, LI JIA‡, ZHONGBO SU‡,
ZHENGMING WAN§ and RENHUA ZHANG†

†Institute of Geographical Sciences and Natural Resources Research, 100101 Beijing, China
‡Alterra Green World Research, 6700 AA Wageningen, The Netherlands
§ICESS, University of California, Santa Barbara, CA 93106-3060, USA

(*Received 7 January 2002; in final form 24 September 2002*)

Abstract. This paper presents a new algorithm to determine quantitatively column water vapour content (W) directly from ATSR2 (Along-Track Scanner Radiometer) Split-Window radiance measurements. First, the Split-Window Covariance-Variance Ratio (SWCVR) method is reviewed. The assumptions made to derive this method are highlighted and its applicability is discussed. Then, an operational use of this method is developed and applied to several ATSR2 datasets. The water vapour contents retrieved using ATSR2 data from SGP'97 (USA), Barrax (Spain) and Cabauw (The Netherlands) are in good agreement with those measured by the quasi-simultaneous radiosonde. The mean and the standard deviation of their difference are $0.04\,g\,cm^{-2}$ and $0.22\,g\,cm^{-2}$, respectively. It is shown that water vapour content derived from ATSR2 data using the proposed algorithm is accurate enough in most cases for surface temperature determination with a split-window technique using ATSR2 data and for atmospheric corrections in visible and near-infrared channels of ATSR2.

1. Introduction

Atmospheric water vapour is a key driver of global circulation. As such, it is of interest in studies involving weather, climate modelling and hydrologic cycles. Water vapour in the atmosphere is also an important greenhouse gas, because it plays a significant role in the absorption and emission of radiative energy. Although the importance of water vapour to a variety of atmospheric processes has been recognized for some time, the poor coverage and representativeness of conventional radiosonde data has both hindered our understanding of the distribution and transport of water vapour and at the same time highlighted the need for satellite-based measurements of water vapour. In addition, the knowledge of water vapour in the atmosphere allows remote sensing scientists to improve the accuracy of the remotely sensed surface parameters (Sobrino *et al.* 1994, Francois and Ottle 1996).

* Present address: TRIO/LSIIT (CNRS UMR 7005), 5 Bld Sebastien Brant, 67400 Illkirch, France; e-mail: li@sepia.u-strasbg.fr

International Journal of Remote Sensing
ISSN 0143-1161 print/ISSN 1366-5901 online
http://www.tandf.co.uk/journals
DOI: 10.1080/0143116031000096014

In response of these needs, a number of different satellite approaches have been proposed and developed over the past two decades to measure atmospheric water vapour. According to the wavelength used, these approaches may be grouped into three categories: near-infrared techniques (Frouin *et al.* 1990, Kaufman and Gao 1992); passive microwave techniques (Prabhakara *et al.* 1985, Alishouse *et al.* 1990, Schulz *et al.* 1993); and thermal infrared techniques (Chesters *et al.* 1983, Susskind *et al.* 1984, Kleespies and McMillin 1990, Jedlovec 1990, Iwasaki 1994, Ottlé *et al.* 1997, Sobrino *et al.* 1999).

Because the near-infrared technique is based on detecting the absorption by water vapour of the reflected solar radiation as it is transferred down to the surface and up through the atmosphere, use of this technique needs to have at least one channel in the water absorption band (0.94 μm), and one nearby channel in the atmospheric windows (0.86 μm, 1.05 μm and 1.24 μm). Since ATSR-2 (Along-Track Scanner Radiometer) on board ERS-2 (European Remote Sensing) has only four channels in the visible and near-infrared domain (0.55 μm, 0.65 μm, 0.87 μm, 1.60 μm) and three channels in the thermal infrared domain (3.7 μm, 11 μm and 12 μm), no channel in the water absorption band is available; the near-infrared technique, therefore, cannot be applied to ATSR2 data and the only one applicable technique is the thermal infrared technique.

Up to now, there have been several attempts to derive water vapour using two split-window channels (11 μm and 12 μm). Thus, Kleespies and McMillin (1990) proposed a method based on the ratio of split-window channel brightness temperature differences, assuming that the atmosphere and surface emissivities in the split-window channels are invariant. Jedlovec (1990) proposed an extension of this concept and showed that the water vapour content can be derived using the ratio of the spatial variance of the channel brightness temperature. On the basis of these methods, Iwasaki (1994) developed a new algorithm to reduce the non-linear effect of air temperature and unresolved cloud effect on the estimation of water vapour content using the split-window data. Sobrino *et al.* (1994) improved Jedlovec's (1990) method by the use of Split-Window Covariance-Variance Ratio (SWCVR). It has been shown that all these split-window methods are sensitive to instrument noise and are difficult to apply to satellite data, such as AVHRR, in an operational manner (Sobrino *et al.* 1994, 1999).

As the thermal infrared data quality is high for ATSR2 (its nominal noise equivalent temperature difference (NEΔT) is only 0.04 K (Bailey 1995)) and the SWCVR method is difficult to use in an operational manner, the general objectives of this work are twofold: (1) to refine the SWCVR method and develop an operational algorithm to retrieve atmospheric water vapour content from split-window radiance measurements; (2) to check whether the water vapour content derived from ATSR2 data is accurate enough for surface temperature determination with the split-window technique and for atmospheric corrections in visible and near-infrared channels of ATSR2. Section 2 presents the principle of the method, while its operational implementation is given in section 3. Finally, a comparison with column water vapour derived from quasi-simultaneous radiosonde data and the impact of error of water vapour on surface parameter retrievals are shown in section 4.

2. Methodology

2.1. *Principle of the method*

On the basis of radiative transfer theory, for a cloud-free atmosphere under local thermodynamic equilibrium, the radiance I_i measured from space in channel i at the zenith view angle θ may be written with a good approximation as (Becker and Li 1990)

$$I_i(\theta) = B_i(T_i(\theta)) = \varepsilon_i(\theta) B_i(T_s) \tau_i(\theta) + R_{ati\uparrow}(\theta) + (1-\varepsilon_i(\theta)) R_{ati\downarrow} \tau_i(\theta). \quad (1)$$

where $T_i(\theta)$ is the brightness temperature in channel i at satellite level at the zenith angle θ, $\varepsilon_i(\theta)$ and $\tau_i(\theta)$ are the directional surface emissivity and total atmospheric transmittance in channel i at the zenith angle θ, respectively, T_s is the surface temperature, $R_{ati\uparrow}(\theta)$ is the atmospheric upwelling radiance at the zenith angle θ and $R_{ati\downarrow}$ is the downwelling hemispheric atmospheric radiance in channel i divided by π.

Under the condition that the atmosphere and directional surface emissivity in channel i are constant or the effects of their spatial variations are not larger than the combined effects of both instrument noise over the N neighbouring pixels and the linear approximation of equation (3), from equation (1), the variation of radiance measured from space in channel i at the zenith angle θ due to the change of surface temperature can be expressed as

$$B_i(T_{i,k}(\theta)) - B_i(\overline{T_i}(\theta)) = \varepsilon_i(\theta) \tau_i(\theta) \left[B_i(T_{s,k}) - B_i(\overline{T_s}) \right] \quad (2)$$

Where the subscript k denotes pixel k, $\overline{T_i}$ and $\overline{T_s}$ are the mean (or the median) brightness temperature and the mean (or the median) surface temperature of the N neighbouring pixels considered, respectively. Since the total numbers of line (m) and column (n) constituting N pixels ($N = m \times n$) are generally small ($n \leq 50$), the variation of zenith view angle ($\Delta\theta$) is very small over N neighbouring pixels ($\Delta\theta \leq 4^\circ$ for AVHRR and ATSR2). Thus, the view angle θ for N neighbouring pixels can be considered as constant; for simplicity, the dependence on view angle in equation (2) will be omitted in the following text.

Considering the first-order Taylor series of the Planck function $B_i(T)$ around some mean temperature $\overline{T}$ in the form

$$B_i(T) \cong B_i(\overline{T}) + \frac{\partial B_i(\overline{T})}{\partial T} (T - \overline{T}), \quad (3)$$

equation (2) can be expressed in terms of temperature difference as

$$(T_{i,k} - \overline{T_i}) = \varepsilon_i \tau_i (T_{s,k} - \overline{T_s}). \quad (4)$$

Similarly, for measurements in channel j, one has

$$(T_{j,k} - \overline{T_j}) = \varepsilon_j \tau_j (T_{s,k} - \overline{T_s}). \quad (5)$$

Dividing equation (5) by equation (4) gives

$$(T_{i,k} - \overline{T_i}) \frac{\tau_j}{\tau_i} \frac{\varepsilon_j}{\varepsilon_i} - (T_{j,k} - \overline{T_j}) = 0. \quad (6)$$

or

$$(T_{j,k} - \overline{T_j}) \frac{\tau_i}{\tau_j} \frac{\varepsilon_i}{\varepsilon_j} - (T_{i,k} - \overline{T_i}) = 0. \quad (7)$$

If the assumption made above holds for N neighbouring pixels, then, by least-squares analysis of equations (6) and (7), the transmittance ratios in two channels,

τ_j/τ_i and its reciprocal, τ_i/τ_j, can be respectively derived from

$$\frac{\tau_j}{\tau_i} = \frac{\varepsilon_i}{\varepsilon_j} R_{ji} \text{ with } R_{ji} = \frac{\sum_{k=1}^{N} \left(T_{i,k} - \overline{T_i}\right)\left(T_{j,k} - \overline{T_j}\right)}{\sum_{k=1}^{N} \left(T_{i,k} - \overline{T_i}\right)^2}, \tag{8}$$

and

$$\frac{\tau_i}{\tau_j} = \frac{\varepsilon_j}{\varepsilon_i} R_{ij} \text{ with } R_{ij} = \frac{\sum_{k=1}^{N} \left(T_{i,k} - \overline{T_i}\right)\left(T_{j,k} - \overline{T_j}\right)}{\sum_{k=1}^{N} \left(T_{j,k} - \overline{T_j}\right)^2}. \tag{9}$$

It is worth noting a number of points.

1. The numerator and denominator on the right-hand side of these equations represent, respectively, the covariance and the variance of the brightness temperature directly measured by the satellite, and the transmittance ratioscan be derived directly from satellite data provided that the emissivity ratio of two channels is known.
2. Equation (8) has the same form as the SWCVR method developed by Sobrino *et al.* (1994); however, operational use of this formula is quite different, as shown below.
3. If r denotes the linear correlation coefficient of two measurements T_i and T_j, from equations (8) and (9), the square of this linear correlation coefficient, r^2, is just the product of R_{ji} and R_{ij}, namely,

$$r^2 = \frac{\left(\sum_{k=1}^{N} \left(T_{i,k} - \overline{T_i}\right)\left(T_{j,k} - \overline{T_j}\right)\right)^2}{\sum_{k=1}^{N} \left(T_{i,k} - \overline{T_i}\right)^2 \sum_{k=1}^{N} \left(T_{j,k} - \overline{T_j}\right)^2} = R_{ji} R_{ij}, \tag{10}$$

and

$$r^2 = R_{ji} R_{ij} = \frac{\varepsilon_j \tau_j}{\varepsilon_i \tau_i} \times \frac{\varepsilon_i \tau_i}{\varepsilon_j \tau_j} = 1. \tag{11}$$

This indicates that the transmittance ratio derived from equations (8) or (9) is feasible only if the brightness temperatures T_i and T_j made in the two split-window channels i and j over N pixels are perfectly correlated ($r = 1$) or almost perfectly correlated ($r \cong 1$). This constraint can be used to check whether the assumptions made in the derivation of equations (8) and (9) are fulfilled.

4. With the aid of the hemispheric spectral reflectance measured in laboratory (Salisbury and D'Aria 1992), emissivity ratios of channels 11 μm and 12 μm ($\varepsilon_{11}/\varepsilon_{12}$) are calculated using the channel filter functions of ATSR2 for different types of natural surface materials including rocks, soils, vegetation, snow and water. Figure 1 shows these emissivity ratios in function of sample number. From this figure, we notice that

   (i) Emissivity ratios of channels 11 μm and 12 μm are between 0.98 and 1.01 for soils, vegetation, snow and water. Because pixels at a scale of 1×1 km

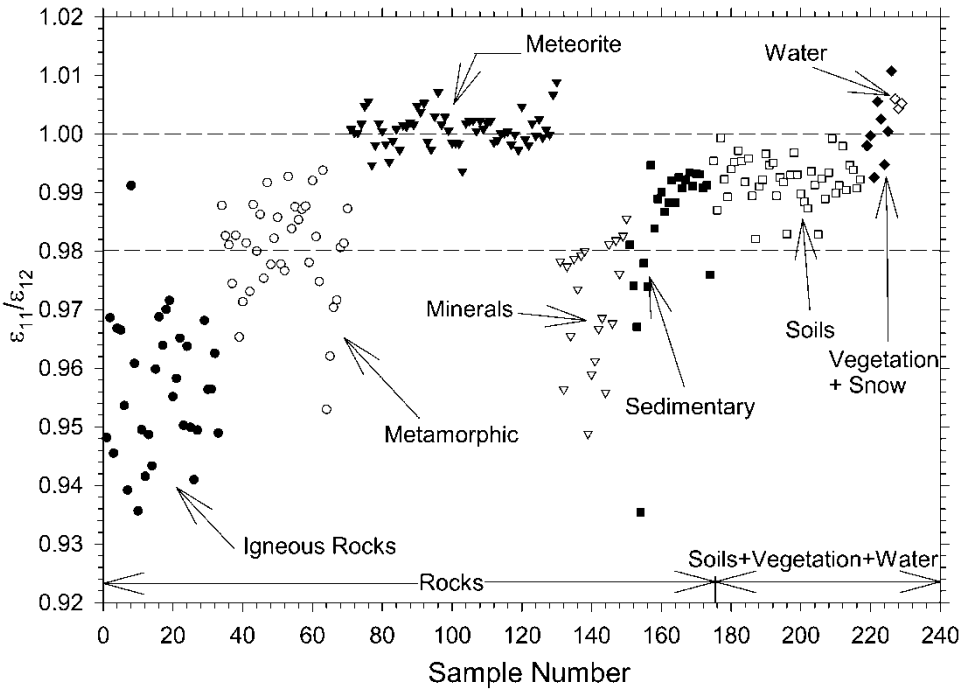

Figure 1. Emissivity ratios ($\varepsilon_{11}/\varepsilon_{12}$) of channels 11 μm and 12 μm of ATSR2 calculated from the hemispheric reflectances measured in laboratory by Salisbury and D'Aria (1992) for different types of natural surfaces.

(like ATSR2 and AVHRR) are generally mixtures of different types of surfaces, in practice, this emissivity ratio is assumed to be unity at this scale (this might be a good approximation for most surfaces), leading to

$$\frac{\tau_j}{\tau_i} \cong R_{ji}. \tag{12}$$

(ii) Emissivity ratios of channels 11 μm and 12 μm are far from unity for igneous and minerals rocks. For these types of surfaces, an emissivity ratio correction in equations (8) and (9) should be performed to get the transmittance ratio correctly. However, for meteorite and most of metamorphic and sedimentary rocks, emissivity ratios of channels 11 μm and 12 μm are between 0.98 and 1.01, therefore, equation (12) might be also a good approximation for these types of surfaces at a scale of 1×1 km.

2.2. *Relationship between transmittance ratio and water vapour content*

The transmittance ratio, either simulated or estimated, provides a relative measure of water vapour content in the atmosphere. Thus a spatial distribution of the SWCVR gives an estimate of the relative horizontal variability in water vapour content in the atmosphere. In order to quantify this variability, it is necessary to form a relationship between column water vapour (W) and the transmittance ratio

(τ_j/τ_i). If we take channel 11 μm of ATSR2 as channel i and channel 12 μm as channel j, the transmittance ratio is always less than unity since the effect of water vapour in channel 12 μm is larger than that in channel 11 μm. The more water vapour content in the atmosphere, the smaller is the transmittance ratio. Therefore, an inverse relationship exists between W and τ_j/τ_i.

Since the atmospheric absorption in the atmospheric window (10–12 μm) is principally due to the water vapour continuum and its absorption coefficient generally depends on temperature and pressure, and particularly on the water vapour partial pressure (Clough *et al.* 1989, Theriaut et al. 1994, Ma and Tipping 1994, Clough 1995), it is therefore difficult – even impossible – to express explicitly these dependences in a simple form. Thus, for the present, the relationship between transmittance ratio and water vapour content is determined by synthetic regression on the simulated data. Channel transmittances are simulated using the commonly used atmospheric transmittance/radiance computer code-MODTRAN 4.0 (Beck *et al.* 1999) with ATSR2 filter response functions for each of 1761 atmospheric profiles. These atmospheric profiles were carefully selected from a global radiosounding dataset (Achard 1991) and were initially used to give the TIROS–N Operational Vertical Sounder (TOVS) initial guess retrievals for atmospheric profile retrievals from satellite vertical sounders (Chedin *et al.* 1985). Figures 2 and 3 display the distribution of total column water vapour content (W) and that of air temperature (T_a) in the first layer of atmosphere for these 1761 selected atmospheres, respectively. These atmospheric profiles represent a world-wide set of atmospheric situations and are obviously credible to derive the relationship between W and τ_{12}/τ_{11} (subscripts 11, 12 denote channel 11 μm and 12 μm, respectively). The transmittance ratio (τ_{12}/τ_{11}) is then regressed against the total column water vapour content W in the atmosphere computed from the 1761 atmospheric profiles. Scatter diagrams and regression coefficients for ATSR2 at nadir view are shown in figure 4, which shows that for a given zenith view angle (θ) water vapour content in the atmosphere (W) is essentially linearly related to the ratio of the two split-window

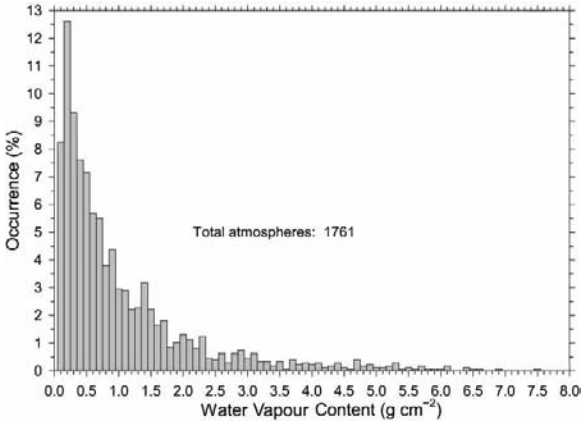

Figure 2. Distribution of the total column water vapour content W in the 1761 atmospheric profiles used to derive the relationship between W and the transmittance ratio in equations (13) and (15).

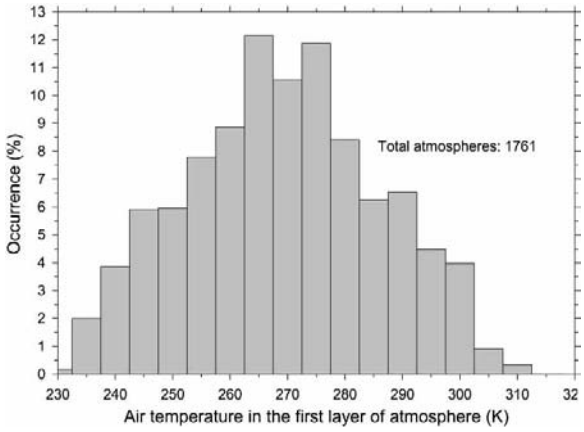

Figure 3. Distribution of the total column water vapour content W in the 1761 atmospheric profiles used to derive the relationship between W and the transmittance ratio in equations (13) and (15), with air temperature in the first layer of atmosphere.

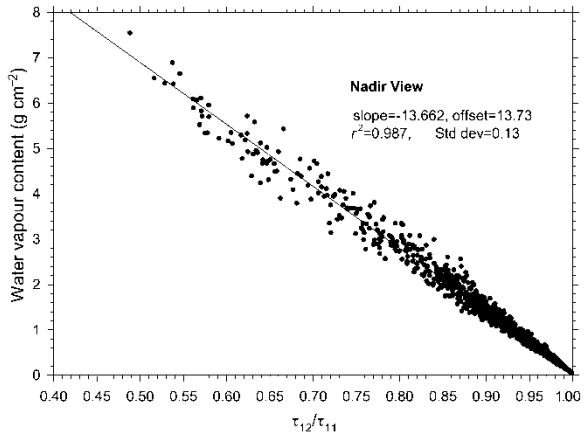

Figure 4. Water vapour content (W) plotted as a function of the transmittance ratio, τ_{12}/τ_{11}, for ATSR2 at nadir view ($\theta \cong 10^\circ$).

channel transmittances (τ_{12}/τ_{11}). Quadratic and logarithmic fits were also tried, but they did not give the better results.

As the variations of the zenith view angle at surface for both ATSR2 nadir and forward views are small (whole variation of θ ranges from 0° to 22° for nadir view and from 52° to 55° for forward view), mean zenith view angle is used in our simulations ($\theta \cong 10^\circ$ and $\theta \cong 53^\circ$ for ATSR2 nadir and forward views, respectively). From the linear regression analysis on the simulated data, for ATSR2 nadir view ($\theta \cong 10^\circ$), we get

$$W = 13.73 - 13.662\tau_{12}/\tau_{11} \tag{13}$$

with a correlation coefficient of 0.987 and a standard deviation error of $0.13\,\mathrm{g\,cm^{-2}}$.

A number of points should be noted.

1. The linear relationship of the type of equation (13) is only a first-order approximation of the relationship between W and τ_{12}/τ_{11}.
2. The discrepancy between the water vapour predicted by the linear regression and the actual water vapour in figure 4 might result from the non-linear effect of the air temperature profile. This effect has been pointed out and discussed by Iwasaki (1994, 1999). Thus, to get a more accurate water vapour content from the ratio of the two split-window channel transmittances, the non-linear effect of the air temperature profile must be taken into account (Iwasaki 1994)
3. The offset and slope in equation (13) are in good agreement with those (offset = 13.85, slope = −13.48) given by Kleespies and McMillin (1990) for AVHRR on-board NOAA7.
4. As shown in figures 2 and 3, the majority of atmospheric profiles are very cold and dry and the statistics shown in figure 4 are, in principle, dominated by these cases containing little water vapour. In order to check how accurate is the linear regression given in equation (13), more moderate and moist atmospheric profiles should be added. Because there are no more atmospheric profiles available to us, instead of including more moderate and moist atmospheres in the statistics, the dry atmospheres with water vapour content less than 1.0 g cm^{-2} are excluded. The new slope and offset of the linear regression applied to the remaining atmospheres (598 atmospheres instead of 1761) are −13.341 and 13.48 respectively. Therefore, the difference of water vapour content derived from these two databases is

$$\Delta W = 0.25 - 0.321\tau_{12}/\tau_{11}. \tag{14}$$

For τ_{12}/τ_{11} ranging from 1.0 to 0.55, which corresponds roughly to W from 0 to 6 g cm^{-2}, ΔW varies from −0.07 to 0.07 g cm^{-2}, which is negligible when comparing with the other errors in the development and application of the method.

Similarly, for ATSR2 forward view ($\theta \cong 53^\circ$), we get

$$W = 10.02 - 9.971\tau_{12}/\tau_{11} \tag{15}$$

with a correlation coefficient of 0.986 and a standard deviation error of 0.13 g cm^{-2}.

It should also be noted that for other instruments, such as AVHRR and MODIS, the zenith view angle at surface varies from 0° to 69°, and the zenith view dependence of the linear regression coefficients must be taken into account. A simple way to perform this is to derive the linear regression coefficients using the simulation data for several view angles, then interpolate these coefficients for any viewing angle.

3. Implementation and application of the method to ATSR2 data

The implementation and application of this technique to ATSR2 data is simple. After the data checking, cloud screening and water area masking procedures, a template (or box) size of $m \times n$ ($N = m \times n$) has to be defined so that various linear regression algorithms (see below) can be applied to each template area. Since the method described above is not applicable to water surface due to the small variation in surface temperature, pixels corresponding to the water surface are

excluded in the calculation procedures. Cloud pixel has a significant impact on the transmittance ratio (Labed *et al.* 1994), therefore, cloud screening is a prerequisite to guarantee accurate water vapour retrieval. A cloud screening algorithm based on Saunder and Kriebel's (1988) threshold method was adapted to ATSR2. Threshold values are subjectively determined for each image based on ATSR2 visible and infrared data. The choice of a template size is initially somewhat arbitrary. The size of template is initially fixed to be 10×10 pixels ($N = 100$, about $100\,\text{km}^2$). The conditions (the atmosphere and emissivity are spatially unchanged but surface temperature changes) under which equations (8) or (9) were derived are most probably held at this size of template ($\cong 100\,\text{km}^2$). These conditions will be checked in step 5. Figure 5 shows a flow diagram of the algorithm to retrieve water vapour content from each template. The steps of this algorithm are presented in sufficient detail to permit regeneration of the processing code after having performed the preprocessing procedures mentioned above. The input ATSR2 data for each template are the brightness temperatures (T_{11}, T_{12}) in the two split-window channels, 11 μm and 12 μm, together with cloud and water surface masks. The output datasets consist of the derived water vapour content and the degree of its reliability. Below is the description of each step involved in the algorithm.

1. Calculating the median values of T_{11} and T_{12} for the template. Of course, pixels having been masked as cloud and water surface are neither included in this calculation nor in the following ones. Here, the median values $\overline{T}_{11}$ and

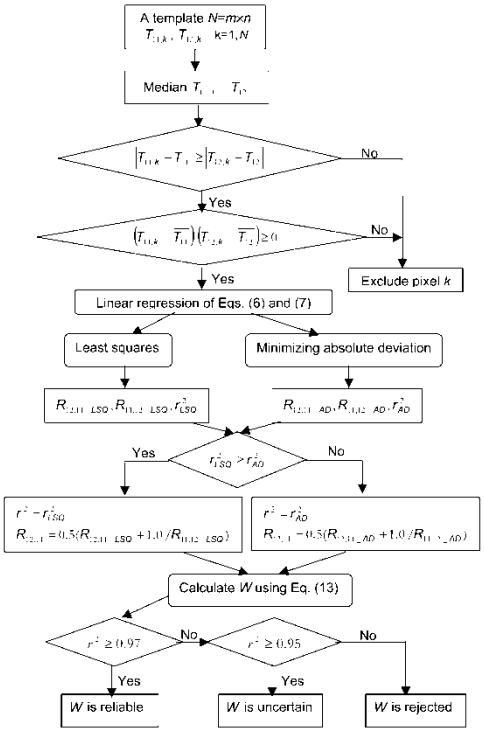

Figure 5. Flow chart of the procedures to retrieve water vapour content from ATSR2 data for a given template.

$\overline{T}_{12}$ are used instead of the mean values not only because the median is a more robust estimator than is the mean, but also because the mean surface temperature $\overline{T}_s$ is channel-dependent (Becker and Li 1995). In our case, two values $\overline{T}_s$ (each for one channel) can exist for one template due to the non-linear dependency of the Planck function on temperature, but there is the only one median value for one template.

2. Removing the abnormal pixels. Since the transmittance in channel at 12 μm (τ_{12}) is smaller than that in channel 11 μm (τ_{11}), τ_{12}/τ_{11} is smaller than unity, as shown in figure 4. Taking into account the fact that the ratio of emissivities in these two channels ($\varepsilon_{12}/\varepsilon_{11}$) at a spatial resolution of $1 \times 1\,\mathrm{km}^2$ is very close to unity, according to equation (6), for common land surfaces, the absolute value of $(T_{11} - \overline{T}_{11})$ must be greater than the absolute value of $(T_{12} - \overline{T}_{12})$, moreover, values of $(T_{11} - \overline{T}_{11})$ and $(T_{12} - \overline{T}_{12})$ should have the same sign. Therefore, pixels for which $\mathrm{abs}(T_{11} - \overline{T}_{11}) < \mathrm{abs}(T_{12} - \overline{T}_{12})$ or $(T_{12} - \overline{T}_{12})(T_{11} - \overline{T}_{12}) < 0$ have to be excluded in the calculation of the transmittance ratios.
3. Estimation of $R_{12,11}$, $R_{11,12}$ and r^2. As predicted by equations (6) and (7), $R_{12,11}$ and its reciprocal, $R_{11,12}$, are the slope of the simple straight line described by equations (6) and (7), respectively. To fit data points to these two straight lines, two linear regression methods are employed. One minimizes the mean square deviation, commonly called linear least-squares method (LSQ method), another minimizes the Absolute Deviation (AD method). The latter one is more robust than the first one if there are outlier points presented in the template because the least-squares fitting have undesired sensitivity to outlying points (Press *et al.* 1992).
4. Selection of the appropriate method to estimate $R_{12,11}$ as well as water vapour content. As discussed following equation (11), only the criterion of measuring the applicability of the method is to check whether the square of the correlation coefficient r^2 ($r^2 = R_{12,11}R_{11,12}$) is close to unity. Ideally, r^2 should be equal to unity as predicted by equation (11). The closer to unity is r^2, the more accurate are $R_{12,11}$ and $R_{11,12}$ retrievals. Thus the method giving the higher r^2 is always selected. That is to say if the r^2 obtained using the LSQ method is greater than that obtained using the AD method, the mean of $R_{12,11}$ and the inverse of $R_{11,12}$ obtained with the LSQ method is used to estimate water vapour content with equation (13), otherwise the mean of $R_{12,11}$ and the inverse of $R_{11,12}$ derived with the AD method is used.
5. Quality assurance. As r^2 should be equal to unity as predicted by equation (11), the value of r^2 can be used to indicate the quality of water vapour retrieval. The closer to unity is r^2, the more accurate are $R_{12,11}$ and $R_{11,12}$ retrievals, which means that the conditions required to derive transmittance ratio are more likely to be satisfied. The degree of this satisfaction depends only on the value of r^2. According to the range of r^2, three rough categories are attributed to each value of water vapour retrieval; reliable if $r^2 \geq 0.97$, and uncertain if $0.95 \leq r^2 < 0.97$, otherwise rejected ($r^2 < 0.95$). At the present, these threshold values are set from our experience. They need to be studied further in the near future.
6. Refining template size for two latter cases (uncertain and rejected cases). The initial size of the template (10×10) is reduced to a smaller size, for example

5×5 to find the sub-templates over which the horizontal homogeneous atmosphere may be assumed (r^2 is close to unity). The algorithm ends when the number of iterations exceeds a limit number or until there is no further improvement for the value of r^2.

4. Results and validation

4.1. *ATSR2 data*

The seventeen ATSR2 datasets used in this study cover three sites and different seasons: 12 datasets of the Barrax site, including the Murcia (39° N, 2° W) and Gibraltar (36° 15′ N, 5° 35′ W) radiosonde locations in Spain; three datasets of the Cabauw site, including De Bilt (The Netherlands), Uccle (Belgium), Trapes and Nancy (France), Hamsby and Herstmonceux (UK), Idar, Emden and Berger (Germany) radiosonde locations; and two datasets of SGP'97 site (36° 6′ N, 97° 5′ W), USA. These three sites were selected because they have distinguished surface properties – the Barrax site, with a sparsely covered surface over most of the study area; the Cabauw site, with nearly fully vegetated surfaces; and the SGP'97 experimental site with mixed surface type – and also because the quasi-simultaneous radiosonde data (within 1h) with ATSR2 data acquisition time are available for these sites.

The standard ATSR2 gridded brightness temperature/reflectance image ($512 \times 512\,\text{km}^2$) was produced for nadir view (view zenith angle at surface, θ, varying from 0° to 22°) and forward view (θ varying from 52° to 55°), co-located and gridded onto a 1 km grid resolution (Bailey 1995).

4.2. *Results and validation*

The algorithm described in section 3 was applied to the images after the cloud-filtering step. The size of the box to calculate $R_{12,11}$ and $R_{11,12}$ in equations (6) and (7) was initially chosen to be 10×10 pixels ($N = 100$). As an example, figures 6(*a*), 6(*b*) and 6(*c*) show the spatial variation of column water vapour content in the atmosphere, its corresponding quality indicator (r^2) and the spatial variation of NDVI (Normalized Difference Vegetation Index), respectively, derived from ATSR2 data ($512 \times 512\,\text{km}^2$) for the Barrax site on 13 April 1999. As shown by the contour lines (black line is 500 m and white line is 1000 m) superimposed on figure 6(*a*), the whole ATSR2 data on 16 April 1999 covers three high mountains located respectively in the south-east of the image (mountain peak is about 3000 m), at the upper left corner (peak is about 2400 m) and at the upper right corner (peak is about 1200 m). Since the method assumes that the atmospheric conditions are invariant for all pixels in a box and changes in topography in the box may lead to changes in water vapour content in the atmosphere, then special consideration should be taken into account over the mountainous regions, as pointed out by Iwasaki (1999). According to the quality indicator (r^2) in figure 6(*b*), only one box in the region (Line 300–350, Column 50–100) is rejected and a few boxes are uncertain, which implies that our algorithm is still applicable to the mountainous regions, at least for this image. As shown in figure 6(*c*), the whole studied image is spatially heterogeneous, covering different types of surface from bare soil (lower NDVI) to fully vegetated surfaces (higher NDVI) and the whole image is likely to be cloud free apart from a few isolated clouds. Comparing it with figure 6(*a*), it seems that there is no evident relationship between the retrieved water vapour and

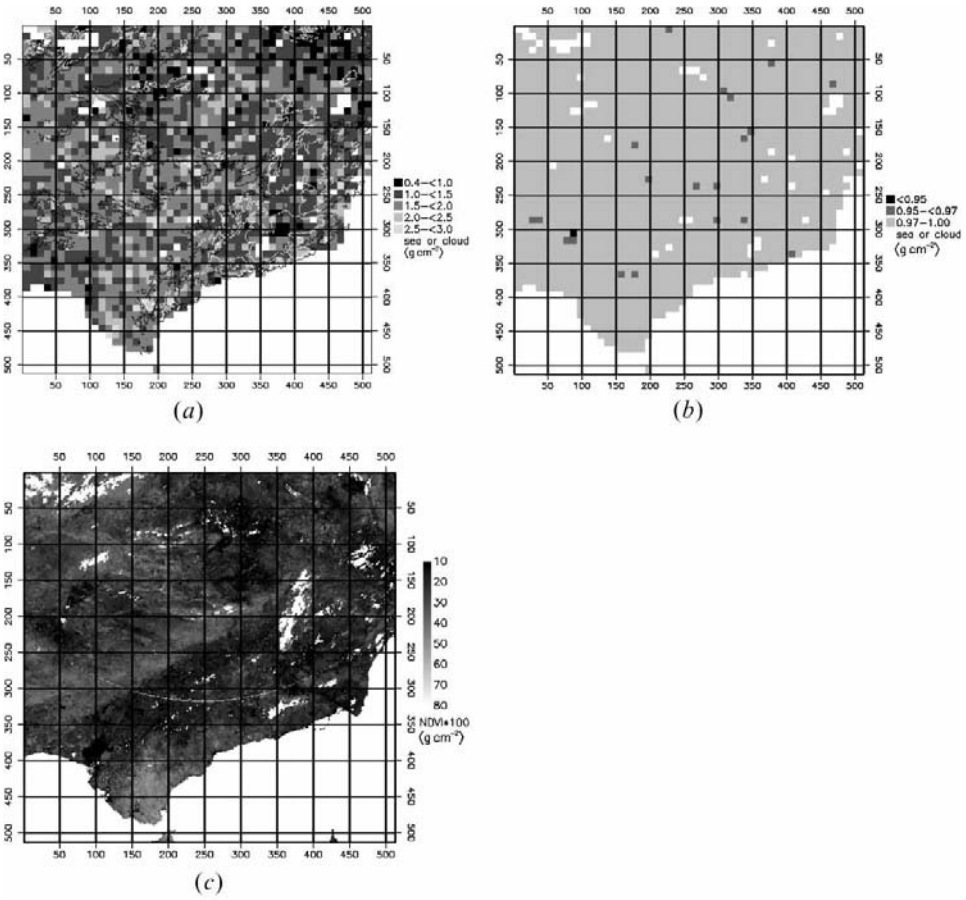

Figure 6. (*a*) Map of the column water vapour content superimposed by contour lines (black contour line is 500 m, white contour line is 1000 m); and (*b*) map of the square of correlation coefficient r^2 (quality of the retrieved water vapour is poor if $r^2 < 0.95$, uncertain if $0.95 \leq r^2 < 0.97$, reliable if $r^2 \geq 0.97$); and (*c*) map of the NDVI (Normalized Difference Vegetation Index). All were obtained from ATSR2 data over the Barrax site on 13 April 1999. Cloud and water surfaces were set to be white in the maps.

the surface types in this image, i.e. the quality of the retrieved water vapour does not depend on the surface types, which implies the good assumption that the surface emissivity ratio in two split-window channels is unity at this scale. A glance at figure 6(*a*) shows that even though the atmosphere in the whole image is relatively dry ($W < 2.5\,\mathrm{g\,cm^{-2}}$ for most regions), we can still recognize two different atmospheres –the relatively moist atmosphere in the valley and plain and the relatively dry atmosphere over the mountains (see also figure 8). Similar results are obtained for other ATSR2 data acquired over the same region (Barrax site), as shown in figure 7 for 16 September 1999. Comparing figure 7 with figure 6(*a*), although the column water vapour contents in the atmosphere are different for both images (column water vapour on 16 September 1999 is relatively higher than that on 13 April 1999), their spatial distributions (patterns) are quite similar for

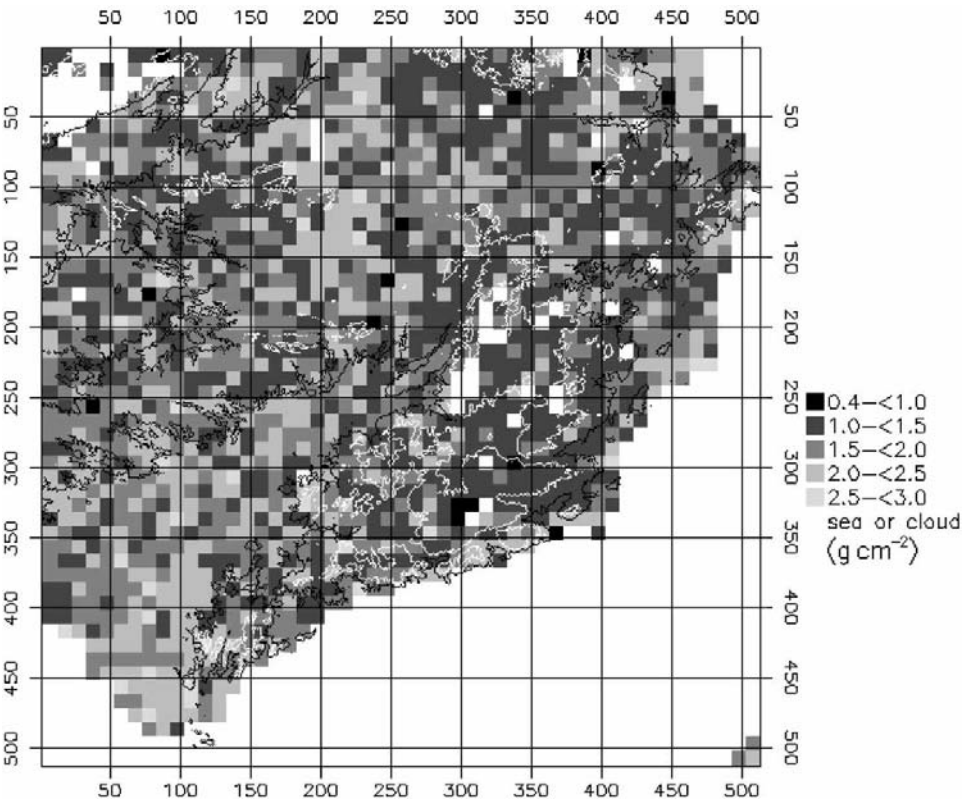

Figure 7. Map of the column water vapour content superimposed by contour lines (black contour line is 500 m, white contour line is 1000 m) on 16 September 1999.

both images at two different seasons. A few isolated boxes in figures 6(*a*) and 7 may be small-scale features of the atmospheric water vapour or noise produced by unresolved clouds, as discussed by Iwasaki (1994) and Labed *et al.* (1994). In order to identify the large spatial-scale feature of the atmospheric water vapour presented in these two images, instead of displaying the full spatial resolution (10×10 km) of water vapour in figures 6(*a*) and 7, coarse spatial resolution images (30×30 km) of water vapour are obtained for these two images by taking the average value of 3×3 boxes in figures 6(*a*) and 7. The spatial distributions of water vapour at coarse resolution are presented in figures 8 and 9. From these two figures, the large spatial-scale features of the atmospheric water vapour observed from figures 6(*a*) and 7 become noticeable, and their spatial distribution patterns are quite similar for both images. Without more additional information, it is difficult to make further investigation.

Figure 10 shows the histograms of the column water vapour for three ATSR scenes ($512\,\text{km} \times 512\,\text{km}$). The histogram of their corresponding r^2 is displayed in figure 11. From these figures, we notice that the column water vapour content in the atmosphere can vary as much as $2.0\,\text{g cm}^{-2}$ over a region of $512 \times 512\,\text{km}^2$ and there are at least 70% of templates having $r^2 \geq 0.97$ (see also table 1)

In order to demonstrate the efficiency of the two constraints ($|(T_{11} - \overline{T}_{11})| \geqslant |(T_{12} - \overline{T}_{12})|$ and $(T_{12} - \overline{T}_{12})(T_{11} - \overline{T}_{11}) > 0$) employed in step 2

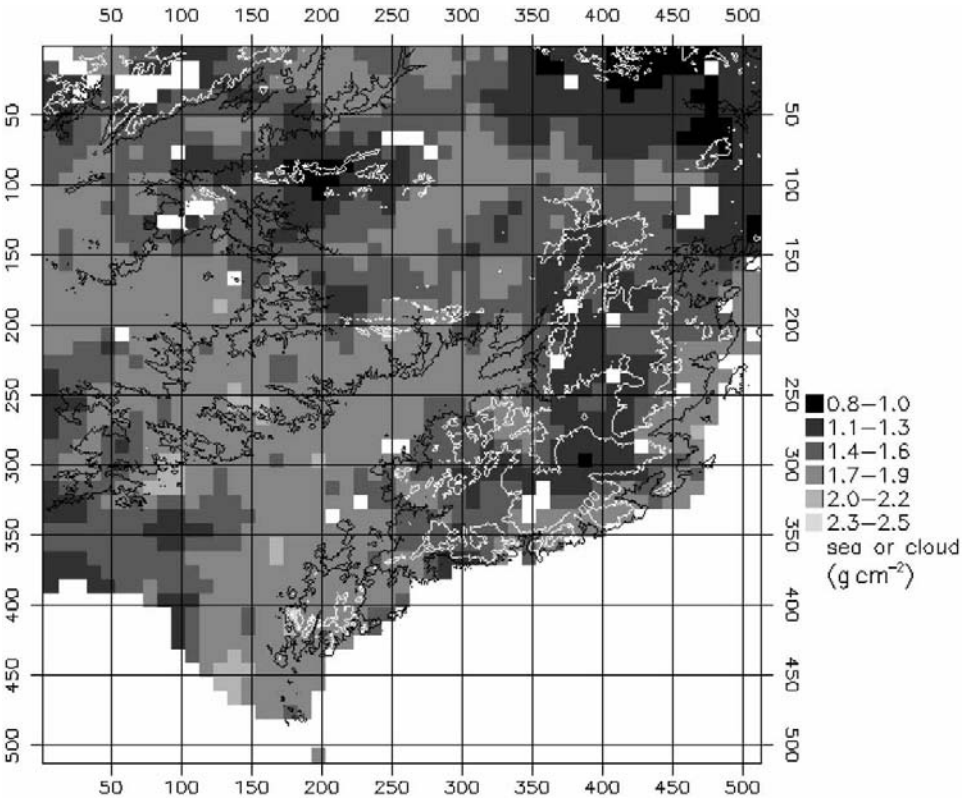

Figure 8. Map of the column water vapour content superimposed by contour lines (black contour line is 500 m, white contour line is 1000 m) with coarse spatial resolution (30 km × 30 km) aggregated by algebraic mean from the fine spatial resolution (10 km × 10 km) shown in figure 6(*a*).

of the proposed algorithm, figure 12(*a*) shows the plot of $(T_{12} - \overline{T}_{12})$ in function of $(T_{11} - \overline{T}_{11})$ over a 10 km × 10 km area at the Murcia site on 8 September 1997. All pixels excluding water and cloud pixels within this area are displayed in this figure. Obviously, the abnormal pixels are presented and contribute to the poor relationship ($r^2 = 0.931$). Scatterplots of the selected pixels at the end of step 2 in the proposed algorithm are shown in figure 12(*b*). As noted, the linear relationship is improved and r^2 increases from 0.931 to 0.981. The difference in linear regression slopes is 0.10 which leads to an error of 1.4 g cm^{-2} in water vapour if equation (13) is used. It should be noted that water vapour content derived using the proposed algorithm for this area is 2.5 g cm^{-2}, and comparison with water vapour measured by radiosonde ($W_{\mathrm{rds}} = 2.34$ g cm^{-2}) indicates that the two constraints used in the proposed algorithm improve the accuracy of water vapour retrievals. Another demonstration is performed to check whether the values of r^2 obtained by the proposed algorithm are increased with respect to other algorithms. Two algorithms are applied to the three scenes of ATSR used previously. One is the algorithm proposed in this paper (denotes Ours), another is the SWCVR method proposed by Sobrino *et al.* (1994), which is the same as Ours, but all available pixels (excluding water and cloud pixels) within a template are used (denoted SWCVR). Table 1 gives

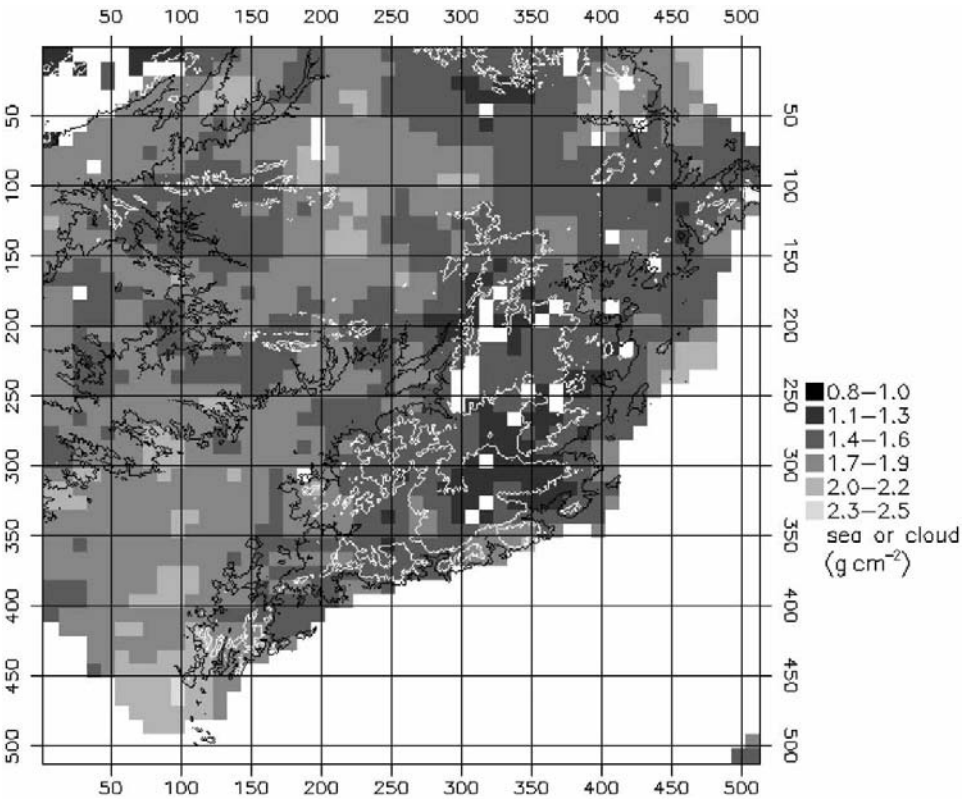

Figure 9. Map of the column water vapour content superimposed by contour lines (black contour line is 500 m, white contour line is 1000 m) on 16 September 1999, with coarse spatial resolution (30 km × 30 km) aggregated by algebraic mean from the fine spatial resolution (10 km × 10 km) shown in figure 7.

the results of this comparison. From this table, we note that the proposed algorithm improves considerably the accuracy of the retrieved transmittance ratio and thus improves the accuracy of W retrievals. For example, for the SGP'97 site, there are only 13.5% of templates having values of r^2 larger than 0.97 if the SWCVR method is used and this is increased to 71.8% if the proposed algorithm (Ours) is employed.

Figure 13 shows the histograms of water vapour derived using the SWCVR method for the three scenes of ATSR used previously. It is noted that negative water vapour content occurs in a few boxes (templates). Examining the spatial distribution of the water vapour content, the boxes with retrieved negative water vapour are found to be either the boxes in the vicinity of a cloudy region or the boxes in which a part of the pixels was cloudy. This may be due to the inappropriate assumption made for the atmosphere in the box (spatially homogeneous atmosphere) or due to the remains of cloudy or partly cloudy pixels in the box after the cloud detection procedure. Comparing with figure 10, we note that the negative water vapour content disappears with the algorithm (Ours) proposed in this paper. This indicates that the proposed algorithm (Ours) can be used to remove the cloudy and partly cloudy pixels.

To validate water vapour content (W_{ATSR}) retrieved from ATSR data, table 2

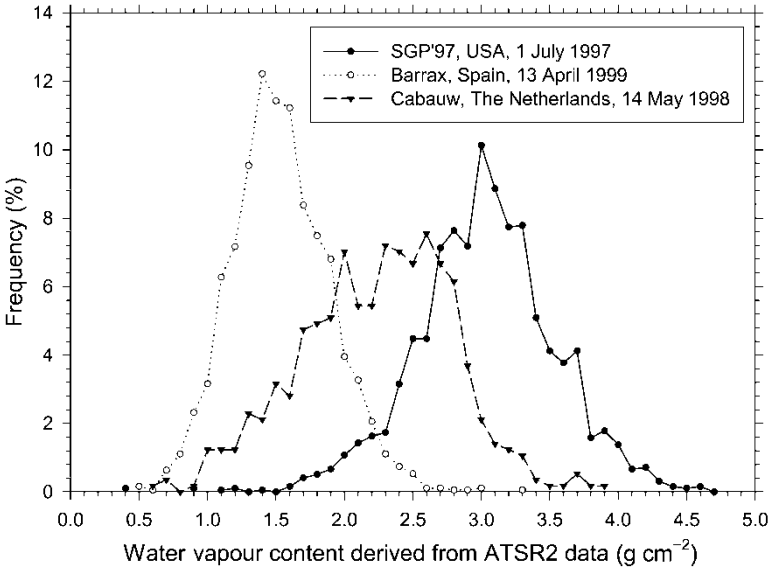

Figure 10. Histograms of the column water vapour content retrieved from ATSR2 data over a zone of $512 \times 512\,km^2$ using the algorithm described in section 3.

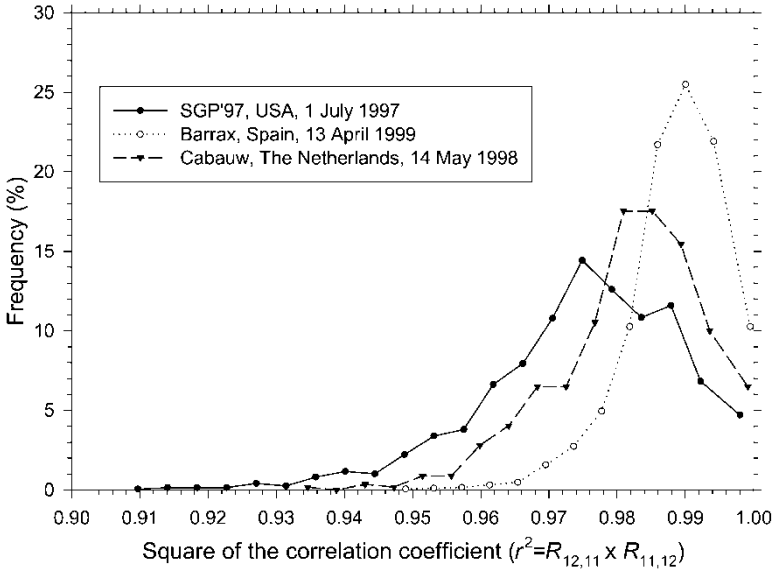

Figure 11. Histograms of the square of correlation coefficient (r^2) derived from ATSR2 data using the algorithm described in section 3. Note that the closer to unity is r^2, the more reliable is the water vapour content determined using the proposed algorithm.

and figure 14 provide a comparison of W measured by radiosonde data (point measurement) denoted W_{rds} (column 4 of table 2) with W_{ATSR} (column 5 of table 2) for a box ($100\,km^2$). From this table and figure, we notice that the W_{ATSR} values retrieved from satellite data are comparable in magnitude with W_{rds} observed by

Table 1. Comparison of the squares of correlation coefficients (r^2) obtained by the algorithm proposed in this paper (denoted Ours) and by the SWCVR method proposed by Sobrino *et al.* (1994).

	Barrax (13 April 1999)		Cabauw (14 May 1998)		SGP'97 (1 July 1997)	
Category	SWCVR	Ours	SWCVR	Ours	SWCVR	Ours
$r^2 \geq 0.97$	66.8	**97.3**	36.5	**84.2**	13.5	**71.8**
$0.95 \leq r^2 < 0.97$	27.5	**2.6**	39.3	**15.1**	33.4	**21.8**
$r^2 < 0.95$	5.7	**0.1**	24.2	**0.7**	53.1	**6.4**

Here the number indicates how many percents of templates in the scene of ATSR2 fall in the given category.

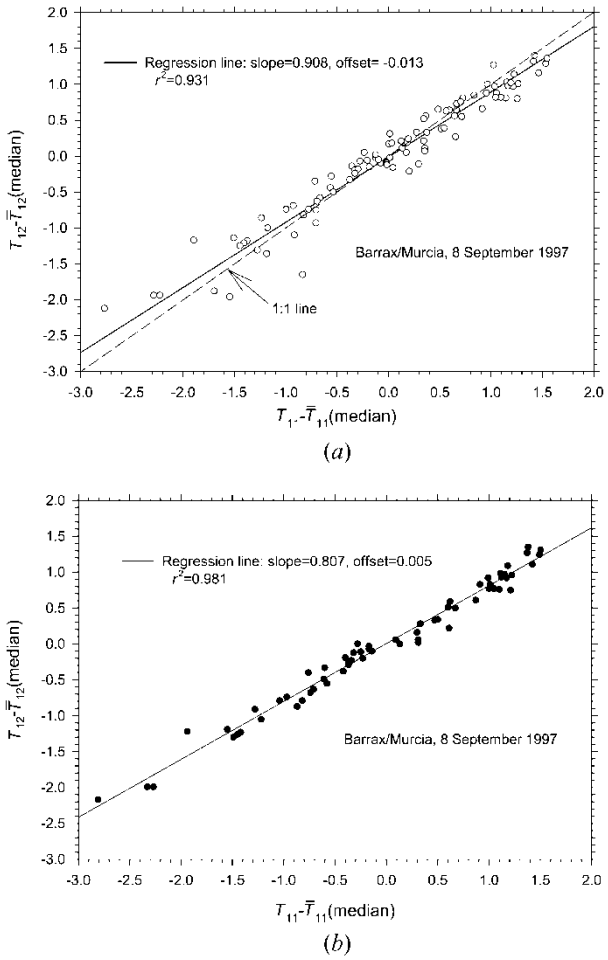

Figure 12. Illustration of the improvement made by the proposed algorithm in determining the transmittance ratio. (*a*) Observed relation from all available pixels (water and cloud pixels are not included) with a $10 \times 10\,\mathrm{km}^2$ area at the Murcia site; (b) the linear relationship defined by the proposed algorithm.

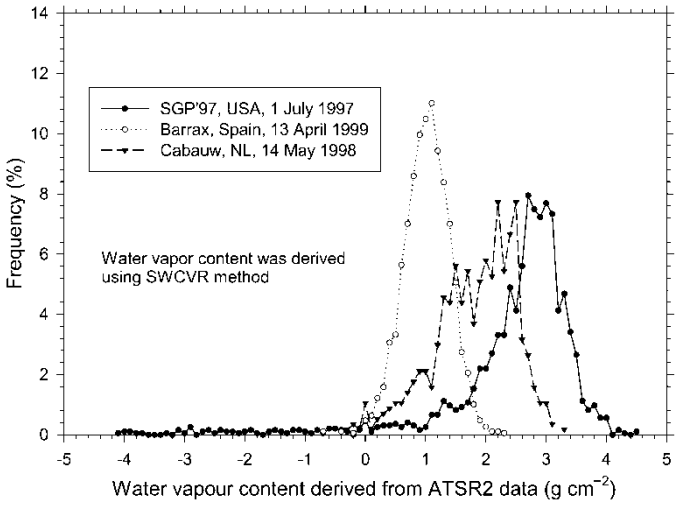

Figure 13. Histograms of the column water vapour content retrieved from ATSR2 data over a zone of $512 \times 512\,\mathrm{km}^2$ using the algorithm described in section 3, deriving the water vapour contents using the SWCVR method.

radio soundings. The mean and the standard deviation of the difference between W_{ATSR} and W_{rds} are $0.10\,\mathrm{g\,cm}^{-2}$ and $0.26\,\mathrm{g\,cm}^{-2}$, respectively. W_{ATSR} exhibits systematically higher values than W_{rds} in SGP'97. This tends to indicate that the atmospheric water vapour content observed by radiosounding is lower than its actual value. In fact, as recognized by the manufacturer (section 3.4.4 at http://www.joss.ucar.edu/data/sgp97/docs/armcart.txt), dry bias has been found in the relative humidity measured by the RS-80H radiosondes used in the SGP'97 experiment. Correction algorithms for this type of dry bias have been developed by several scientists (Lesht 1999, Miller *et al.* 1999, among others). For lack of auxiliary data, we are not able to correct SGP'97 radiosonde data. It should be also noted that the mean and the standard deviation given above become $0.04\,\mathrm{g\,cm}^{-2}$ and $0.22\,\mathrm{g\,cm}^{-2}$ if the data in SGP'97 are excluded.

4.3. *Impact of the error of* W_{ATSR} *on surface temperature and reflectance retrievals*

It is well known that column water vapour in the atmosphere plays an important role in atmospheric corrections in the visible, near-infrared and thermal infrared domains. Methods of atmospheric correction in the visible and near-infrared channels are generally concerned with the estimation of atmospheric effects associated with molecular absorption, molecular and aerosol scattering. Current methods for the estimation of atmospheric effects employ a radiative transfer model (Rahman and Dedieu 1994, Vermote *et al.* 1997) whose inputs are generally the vertically integrated gaseous contents, aerosol optical properties and geometric conditions. The visible and near-infrared channels of ATSR2 have been selected to avoid the molecular absorption bands. Their central wavelengths are $0.55\,\mu\mathrm{m}$, $0.65\,\mu\mathrm{m}$, $0.87\,\mu\mathrm{m}$, $1.60\,\mu\mathrm{m}$ and their corresponding full widths at half maximum are $0.02\,\mu\mathrm{m}$ for the first three channels and $0.06\,\mu\mathrm{m}$ for the last channel. Thus, the molecular

Table 2. Comparison of column water vapour content measured by radiosonde data (W_{rds}, column 4) with collocated W_{ATSR} (column 5) estimated from ATSR data using proposed algorithm for different seasons and different regions.

Sites	Site coordinates	Date	W_{rds} ($g\,cm^{-2}$)	W_{ATSR} ($g\,cm^{-2}$)	W_{ATSR}–W_{rds} ($g\,cm^{-2}$)	r^2
South Great	38° 305′ N, 97° 301′ W	1997.07.01	2.56	3.1	0.54	0.976
Plain, 1997	38° 687′ N, 95° 856′ W		2.86	3.3	0.44	0.970
(SGP'97)	36° 605′ N, 97° 485′ W		2.52	2.9	0.38	0.974
	34° 969′ N, 97° 415′ W	1997.07.02	2.52	3.0	0.48	0.971
	35° 687′ N, 95° 856′ W		3.08	3.7	0.62	0.951
Cabauw						
De Bilt	52° 10′ N, 5° 18′ E	1997.08.17	2.45	2.3	−0.15	0.991
		1997.08.20	2.86	2.8	−0.06	0.991
		1998.05.14	1.58	1.8	0.22	0.999
Uccle	50° 80′ N, 4° 35′ E	1997.08.17	2.38	2.5	−0.12	0.994
		1997.08.20	2.28	2.4	−0.12	0.997
		1998.05.14	2.18	2.0	−0.18	0.999
Trappes	48° 76′ N, 2° 02′ E	1997.08.17	2.49	2.6	0.11	0.989
		1997.08.20	2.19	2.4	0.21	0.976
Nancy	48° 68′ N, 6° 22′ E	1997.08.17	1.94	2.1	0.16	0.998
Hemsby	52° 16′ N, 1° 68′ E	1997.08.20	2.36	2.6	0.24	0.992
		1998.05.14	1.71	2.3	0.59	0.970
Herstmon.	50° 90′ N, 0° 32′ E	1997.08.20	3.04	2.6	−0.44	0.984
Idar	49° 70′ N, 7° 33′ E	1997.08.17	2.19	2.0	−0.19	0.974
		1997.08.20	2.06	1.9	−0.16	0.990
Emden	53° 80′ N, 7° 23′ E	1997.08.20	3.05	3.1	0.05	0.989
Bergen	52° 49′ N, 9° 59′ E	1997.08.17	2.44	2.7	0.26	0.987
Barrax						
Murcia	38° 00′ N, 1° 17′ W	1997.08.07	2.24	2.4	0.16	0.988
		1997.08.20	2.07	2.1	0.03	0.988
		1997.09.05	2.31	2.2	−0.11	0.984
		1997.09.08	2.34	2.5	0.16	0.981
		1997.10.16	1.32	1.3	0.02	0.991
		1998.09.09	2.22	2.4	0.18	0.993
		1999.04.13	1.16	1.0	−0.16	0.993
		1999.06.19	2.08	1.7	−0.38	1.000
		1999.08.28	2.68	2.7	0.02	0.994
		1999.09.16	1.37	1.1	−0.27	1.000
Gibraltar	36° 15′ N, 5° 35′ W	1998.09.15*	2.35	2.4	0.05	0.986
		1999.04.13	1.17	1.4	0.23	0.994
		1999.06.06*	1.18	1.1	−0.08	0.997
		1999.06.19	1.89	2.3	0.41	0.989
		1999.08.28	2.04	2.1	0.06	0.988
		1999.09.16	1.82	1.9	0.08	0.993

*Denotes the site Barrax/Murcia is either cloudy or out of the image frame.

absorption effect is very small and behaves only as a correction factor. As shown in Li *et al.* (2001a), water vapour has a bigger effect on the ATSR2 channel at 0.65 μm than on other channels. Therefore, we use this channel (the worst one) to show the impact of water vapour error on atmospheric corrections through the error introduced in water vapour transmittance. Following the procedure described in Rahman and Dedieu (1994), water vapour transmittance in channel i (τ) can be

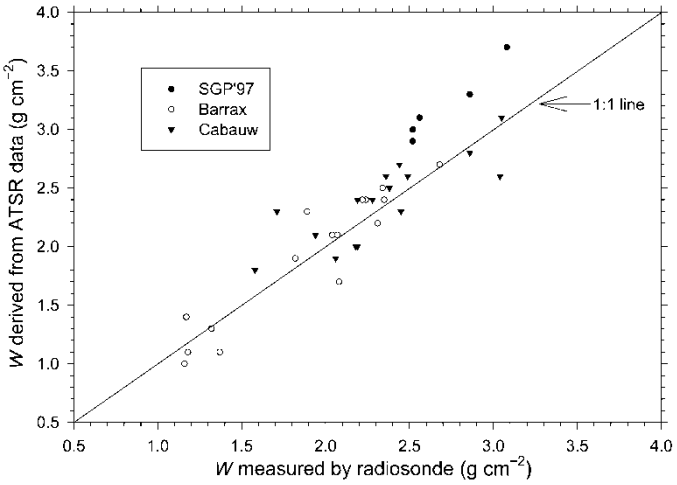

Figure 14. Comparison of water vapour contents derived from ATSR data with those measured by the quasi-simultaneous radiosonde.

approximated by

$$\tau = e^{-a(m \times W)^b}. \tag{16}$$

where a and b are channel constants ($a = 5.38 \times 10^{-3}$, $b = 0.8031$ for the ATSR2 channel at 0.65 μm given by Li *et al.* 2001a), m is the airmass given by

$$m = 1/\cos\theta_s + 1/\cos\theta \tag{17}$$

in which θ_s and θ are solar zenith angle and viewing zenith angle, respectively. Thus, from equation (16), error introduced to the transmittance $\delta\tau$ due to the error in W, δW can be given by

$$\delta\tau/\tau = -ab(mW)^b \delta W/W \tag{18}$$

Inserting typical values of W ($W = 2.0$) and m ($m = 3.7$ for $\theta = 55^\circ$ and $\theta_s = 60^\circ$) in equation (18), one gets $\delta\tau \cong -0.01\delta W$. Consequently, in order to get the accuracy of water vapour transmittance better than 1%, the error on water vapour should be less than 1 g cm^{-2} which is easily attainable by the proposed method, as illustrated in section 4.2.

As for atmospheric corrections in thermal infrared, one of the most popular methods used is called the Split-Window method (Becker 1987, Prata 1993). Assuming that the surface brightness temperature (T_g) is independent of the channels used to measure it, following the procedure developed by Becker and Li (1995), a general SW algorithm is derived by Li *et al.* (2001b) for ATSR-2 nadir and forward views using the simulation data, namely

$$T_g(\theta) = [a(\theta) + b(\theta)W] + [c(\theta) + d(\theta)W]T_{11}(\theta) + [e(\theta) + f(\theta)W][T_{11}(\theta) - T_{12}(\theta)] \tag{19}$$

where the coefficients *a–f* are constant for a large range of surface parameters and atmospheric conditions, $a = -4.89$, $b = 3.74$, $c = 1.0205$, $d = -0.0151$, $e = 0.916$, $f = 0.509$ and the rms. residual retrieval error $\sigma = 0.10K$ for ATSR2 nadir image, and $a = -14.41$, $b = 8.51$, $c = 1.0582$, $d = -0.0343$, $e = 0.565$, $f = 0.857$, $\sigma = 0.24K$ for ATSR2 forward view. On the basis of this equation, error on the retrieved surface

brightness temperature (δT_g) raised by error of water vapour is straightforwardly derived

$$\delta T_g(\theta) = \{b(\theta) + d(\theta)T_{11}(\theta) + f(\theta)[(T_{11}(\theta) - T_{12}(\theta)]\}\delta W \quad (20)$$

Inserting typical values of T_{11} ranging from 295 K to 305 K and T_{11}–T_{12} ranging from 1 K to 3 K, the variation of δT_g is thus from $-0.4\delta W$ to $0.8\delta W$ for nadir view and from $-1.0\delta W$ to $1.0\delta W$ for forward view. Consequently, to get an accuracy of T_g better than 0.5 K, the error on water vapour has to be less than 0.5 g cm^{-2} which is quite feasible with the proposed method. Therefore, it can be concluded at this point that water vapour content derived from ATSR2 data using the proposed method is accurate enough for surface temperature determination with a split-window technique and for atmospheric corrections in the visible and near-infrared channels of ATSR2.

5. Summary and conclusions

A new algorithm is developed for quantitative determination of column water vapour content from ATSR Split–Window radiance measurements. First, it is theoretically shown that the transmittance ratio τ_{12}/τ_{11} (subscripts 11, 12 denote channels 11 μm and 12 μm, respectively) can be expressed by the split-window covariance and variance ratio that can be directly estimated from ATSR Split-Window radiance measurements. Then, a simple linear relationship is derived for water vapour content as a function of the transmittance ratio, τ_{12}/τ_{11}, based on MODTRAN 4.0 simulations using ATSR-2 filter response functions for dry atmosphere to moist atmosphere. The water vapour contents (W) derived from ATSR are then compared with W measured by radiosoundings for different locations and different seasons. The mean and standard deviations of their difference are 0.04 g cm^{-2} and 0.22 g cm^{-2}, respectively. More validation will be made in other sites in the future. Based on the error analysis, it is shown that water vapour content derived from ATSR2 data using the proposed method is accurate enough in most cases for surface temperature determination with a split-window technique and for atmospheric corrections in the visible and near-infrared channels of ATSR2.

Acknowledgments

We are grateful to the British Atmospheric Data Center which provided us with access to the Met Office Radiosonde Data. Part of this work has been funded by the Association Franco-Chinoise pour la Recherche Scientifique et Technique (AFCRST) under contract PRA-E98-02 and by the Dutch Remote Sensing Board (BCRS, reference: 4.2/AP-11.), the Dutch Ministry of Agricultural, Fishery and Nature (LNV, GIS/RS programme) and the Royal Netherlands Academy of Science (KNAW). Dr Wan is supported by NASA EOS program contract NAS5-31370. We thank two anonymous reviewers for their helpful and stimulating comments that greatly improved the quality of the manuscript.

References

ACHARD, V., 1991, *Trois problèmes clés de l'analyse 3D de la structure thermodynamique de l'atmosphère par satellite: measure du contenu en ozone; classification des masses d'air; modélisation 'hyper' rapide du transfert radiatif* (PhD thesis, University of Paris 7), pp. 44–58.

ALISHOUSE, J. C., SNYDER, S. A., VONGSATHORN, J., and FERRARO, R. R., 1990, Determination of oceanic total precipitable water from the SSM/I. *IEEE Transactions on Geoscience and Remote Sensing*, **28**, 811–816.

BAILEY, P., 1995, SADIST-2 v100 products. ER-TN-RAL-AT-2164, Space Science Department, Rutherford Appleton Laboratory, URL http://www.atsr.rl.ac.uk/software.html.

BECK, A., ANDERSON, G. P., ACHARYA, P. K., CHETWYND, J. H., BERNSTEIN, L. S., SHETTLE, E. P., MATTHEW, M. W., and ADLER-GOLDEN, S. M., 1999, *MODTRAN4 User's Manual* (Hanscom AFB, MA: Air Force Research Laboratory).

BECKER, F., 1987, The impact of spectral emissivity on the measurement of land surface temperature from a satellite. *International Journal of Remote Sensing*, **10**, 1509–1522.

BECKER, F., and LI, Z-L., 1990, Temperature independent spectral indices in thermal infrared bands. *Remote Sensing of Environment*, **32**, 17–33.

BECKER, F., and LI, Z-L., 1995, Surface temperature and emissivity at various scales: Definition, measurement and related problems. *Remote Sensing Reviews*, **12**, 225–253.

CHEDIN, A., SCOTT, N. A., WAHICHE, C., and MOULINIER, P., 1985, The Improved Initialization Inversion method: a high resolution physical method for temperature retrievals from satellites of the TIROS-N series. *Journal of Climate and Applied Meteorology*, **24**, 128–143.

CHESTERS, D., UCCELLINI, L. W., and ROBINSON, P., 1983, Low-level water vapor fields from the VISSR atmospheric sounder (VAS) split-window channels. *Journal of Climate and Applied Meteorology*, **22**, 725–743.

CLOUGH, S. A., 1995, The water vapor continuum and its role in remote sensing. *Proceeding of the Conference in Optics. Remote Sensing Atmosphere*, Salt Lake City, UT, pp. 76–78.

CLOUGH, S. A., KNEIZYS, F. X., and DAVIES, R. W., 1989, Line shape and the water vapor continuum. *Atmosphere Research*, **23**, 229–241.

FRANCOIS, C., and OTTLE, C., 1996, Atmospheric corrections in the thermal infrared: global and water vapor dependent split-window algorithm. Application to ATSR and AVHRR data. *IEEE Transactions on Geoscience and Remote Sensing*, **34**, 457–471.

FROUIN, R., DESCHAMPS, P-Y., and LECOMTE, P., 1990, Determination from space of atmospheric total water vapor amounts by differential absorption near 940 nm: Theory and airborne verification. *Journal of Applied Meteorology*, **29**, 448–460.

IWASAKI, H., 1994, Estimation of precipitable water over land using the split-window data from the NOAA satellite. *Journal of the Meteorological Society of Japan*, **72**, 223–233.

IWASAKI, H., 1999, Case study on the distribution of precipitable water associated with local circulation using the split-window data of a NOAA satellite. *Journal of the Meteorological Society of Japan*, **77**, 711–719.

JEDLOVEC, G. J., 1990, Precipitable water estimation from high-resolution split window radiance measurements. *Journal of Applied Meteorology*, **29**, 863–876.

KAUFMAN, Y. J., and GAO, B-C., 1992, Remote sensing of water vapor in the near IR from EOS/MODIS. *IEEE Transactions on Geoscience and Remote Sensing*, **30**, 871–884.

KLEESPIES, T. J., and MCMILLIN, L. M., 1990, Retrieval of precipitable water from observations in the split window over varying surface temperature. *Journal of Applied Meteorology*, **29**, 851–862.

LABED, J., LI, Z-L., and STOLL, M. P., 1994, Land surface temperature retrieval from ATSR data over the Niamey (Niger) area. *Proceedings Second ERS-1 Symposium – Space at the Service of our Environment* (ESA SP361), pp. 389–392.

LESHT, B. M., 1999, Reanalysis of radiosonde data from the 1996 and 1997 water vapor intensive observation periods: Application of the Vaisala RS-80H contamination correction algorithm to dual-sonde soundings. *Ninth ARM Science Team Meeting Proceedings*, San Antonio, Texas, (http://www.arm.gov/docs/documents/technical/conf_9903/lesht-99.pdf).

LI, Z-L., JIA, L., and SU, Z., 2001a, Retrieval of aerosol optical depth from ATSR2 data for atmospheric corrections. In *ENVISAT-Land Surface Processes*, National Remote Sensing Programs Series, edited by Z. Su and G. Roerink, USP-2, 01–07, pp. 17–22.

LI, Z-L., JIA, L., and SU, Z., 2001b, Estimation of vegetation and soil component

temperatures from ATSR2 data. In *ENVISAT-Land Surface Processes*, National Remote Sensing Programs Series, edited by Z. Su and G. Roerink, USP-2, 01–07, pp. 43–54.

MA, Q., and TIPPING, R., 1994, The detailed balance requirement and general empirical formalisms for continuum absorption. *Journal of Quantitative Spectroscopy Radiation Transfer*, **51**, 751–757.

MILLER, E. R., WANG, J., and COLE, H. L., 1999, Correction for dry bias in Vaisala radiosonde RH data. *Ninth ARM Science Team Meeting Proceedings*, San Antonio, Texas, March 22–29, (http://www.arm.gov/docs/documents/technical/conf_9903/miller-er-99.pdf).

OTTLÉ, C., OUTALHA, S., FRANCOIS, C., and LE MAGUER, S., 1997, Estimation of total atmospheric water vapor content from split-window radiance measurements. *Remote Sensing of Environment*, **61**, 410–418.

PRABHAKARA, C., CHANG, H. D., and CHANG, A. T. C., 1985, Remote sensing of precipitable water over the oceans from NIMBUS 7 microwave measurements. *Journal of Applied Meteorology*, **21**, 59–68.

PRATA, A. J., 1993, Land surface temperatures derived from the AVHRR and ATSR, 1 Theory. *Journal of Geophysical Research*, **98**, 16 689–16 702.

PRESS, H. P., TEUKOLSKY, S. A., VETTERLING, W. T., and FLANNERY, B. P., 1992, *Numerical Recipes In C: The Art of Scientific Computing*, 2nd edn (Cambridge University Press).

RAHMAN, H., and DEDIEU, G., 1994, SMAC: a simplified method for the atmospheric correction of satellite measurements in the solar spectrum. *International Journal of Remote Sensing*, **15**, 123–143.

SALISBURY, J. W., and D'ARIA, D. M., 1992, Emissivity of terrestrial materials in the 8–14 μm atmospheric window. *Remote Sensing of Environment*, **42**, 83–106.

SAUNDER, R. W., and KRIEBEL, K. T., 1988, An improved method for detecting clear sky and cloudy radiances from AVHRR data. *International Journal of Remote Sensing*, **9**, 123–150.

SCHULZ, J., SCHLUESSEL, P., and GRASSL, H., 1993, Water vapor in the atmospheric boundary layer over oceans from SSM/I measurements. *International Journal of Remote Sensing*, **14**, 2773–2789.

SOBRINO, J. A., LI, Z-L., STOLL, M. P., and BECKER, F., 1994, Improvement in the split window technique for land surface temperature determination. *IEEE Transactions on Geoscience and Remote Sensing*, **32**, 243–253.

SOBRINO, J. A., RAISSOUNI, N., SIMARRO, J., NERRY, F., and PETITCOLIN, F., 1999, Atmospheric water vapor content over land surfaces derived from AVHRR data: Application to the Iberian Peninsula. *IEEE Transactions on Geoscience and Remote Sensing*, **37**, 1425–1434.

SUSSKIND, J., REUTER, D., and CHAHINE, M. T., 1984, Remote sensing of weather and climate parameters from HIRS2/MSU on TIROS-N. *Journal of Geophysical Research*, **89**, 4677–4697.

THERIAULT, J-M., RONEY, P. L., ST.-GERMAIN, D., REVERCOMB, H. E., KNUTESON, R. O., and SMITH, W. L., 1994, Analysis of the FASCODE model and its H2O continuum based on long-path atmospheric transmission measurements in the 4.5–11.5 μm region. *Applied Optics*, **33**, 323–333.

VERMOTE, E. F., TANRE, D., DEUZE, J. L., HERMAN, M., and MORCRETTE, J. J., 1997, Second simulation of the satellite signal in the solar spectrum, 6S: An overview. *IEEE Transactions on Geoscience and Remote Sensing*, **35**, 675–686.